Available online at www.sciencedirect.com
ScienceDirect
Journal of Power Sources 164 (2007) 510–518
JOURNAL OF POWER SOURCES
www.elsevier.com/locate/jpowsour

Y-doped $SrTiO_3$ based sulfur tolerant anode for solid oxide fuel cells

Hideto Kurokawa *, Liming Yang, Craig P. Jacobson, Lutgard C. De Jonghe, Steven J. Visco

Materials Sciences Division, Lawrence Berkeley National Laboratory, 1 Cyclotron Road, Building R0203, Berkeley, CA 94720, United States

Received 29 September 2006; received in revised form 22 November 2006; accepted 23 November 2006

Abstract

A solid oxide fuel cell (SOFC) anode with high sulfur tolerance was developed starting from a Y-doped $SrTiO_3$ (SYTO)-yttria stabilized zirconia (YSZ) porous electrode backbone, and infiltrated with nano-sized catalytic ceria and Ru. The size of the infiltrated particles on the SYTO-YSZ pore walls was 30–200 nm, and both infiltrated materials improved the performance of the SYTO-YSZ anode significantly. The infiltrated ceria covered most of the surface of the SYTO-YSZ pore walls, while Ru was dispersed as individual nano-particles. The performance and sulfur tolerance of a cathode supported cell with ceria- and Ru-infiltrated SYTO-YSZ anode was examined in humidified H_2 mixed with H_2S. The anode showed high sulfur tolerance in 10–40 ppm H_2S, and the cell exhibited a constant maximum power density 470 mW cm^{-2} at 10 ppm H_2S, at 1073 K. At an applied current density 0.5 A cm^{-2}, the addition of 10 ppm H_2S to the H_2 fuel dropped the cell voltage slightly, from 0.79 to 0.78 V, but completely recovered quickly after the H_2S was stopped. The ceria- and Ru-infiltrated SYTO-YSZ anode showed much higher sulfur tolerance than conventional Ni-YSZ anodes.
Published by Elsevier B.V.

Keywords: Solid oxide fuel cells; Sulfur tolerant anode; Y-doped $SrTiO_3$; Catalyst infiltration

1. Introduction

Solid oxide fuel cells (SOFCs) have been studied as a promising energy conversion and generating system due to their high efficiency, low emissions, and their potential for co-generation. A significant advantage of the relatively high operating temperature of SOFCs is that it enables the use not only of hydrogen but also of a variety of hydrocarbons as well as carbon monoxide. However, practical fuels such as natural gas are likely to expose the anode materials to significant sulfur levels, as well as to carbon deposition, leading to catalysis inhibition.

Traditional Ni-yttria stabilized zirconia (YSZ) anodes have been used in SOFCs for decades, but these anodes are only able to tolerate sulfur concentration at the ppm level. The sulfur impurities, which are present primarily as hydrogen sulfide (H_2S), are expected to have the greatest impact on SOFC performance and lifetime [1]. Geyer et al. [2] measured impedance spectra of Ni-YSZ anodes with and without 5 ppm H_2S in hydrogen and concluded that the polarization resistance for a Ni-YSZ cermet anode doubled at 5 ppm H_2S, at 1223 K. Primdahl and Morgensen [3] reported that poisoning of the Ni surface by 35 ppm H_2S caused a 60% increase in polarization resistance, and may be fully reversible at 1123 and 1273 K. Matsuzaki and Yasuda [4] studied the effect of sulfur (H_2S) on the electrochemical properties of Ni-based anodes by cell impedance analysis at 1023–1273 K. They concluded the poisoning effect became more significant at lower operating temperatures, and the time needed for recovery increased with decreasing operating temperature. Ni-based anodes would recover from sulfur poisoning, but this recovery took 360 ks when the cell had been exposed to as little as 0.05 ppm H_2S at 1023 K. Sasaki et al. [5] also showed that sulfur poisoning becomes serious with increasing H_2S concentration and decreasing operating temperature. They concluded that sulfur poisoning of Ni based anodes consists of at least two states, i.e., an quick initial cell voltage drop to a (meta)stable cell voltage, followed by a gradual and fatal cell voltage drop associated with the accelerated agglomeration of Ni particles.

Low and intermediate temperature SOFCs have received more attention recently due to the less severe requirements for materials compatibilities at higher temperature. As a result, reducing the SOFC operating temperature may greatly lower fabrication and material cost. Since sulfur tolerance of traditional Ni-YSZ anodes drops down drastically at lower temperatures,

* Corresponding author. Tel.: +1 510 486 5195; fax: +1 510 486 4881.
E-mail address: hkurokawa@lbl.gov (H. Kurokawa).

0378-7753/$ – see front matter. Published by Elsevier B.V.
doi:10.1016/j.jpowsour.2006.11.048

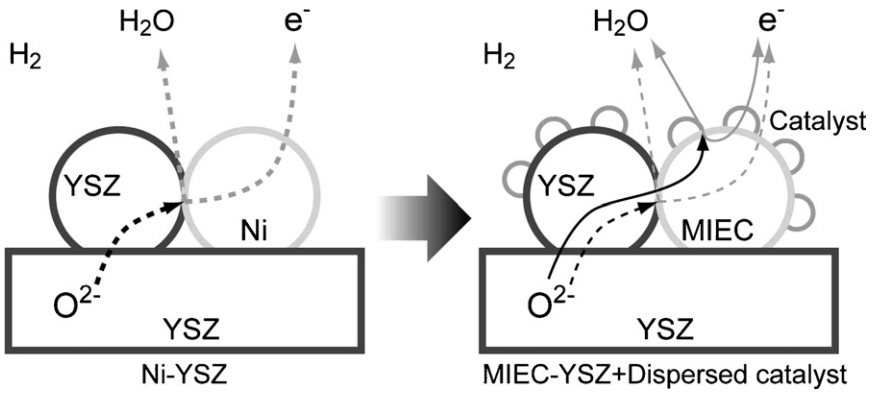

Fig. 1. An alternative design for sulfur tolerant anode with mixed ionic and electronic conductor (MIEC) and dispersed catalyst.

alternative sulfur tolerant anodes are needed to allow the direct use of practical fuels, without the need for extensive reforming and fuel conditioning. Several candidates for alternative anode materials have been studied. Sulfur tolerance was improved by using Sc_2O_3-doped ZrO_2 instead of YSZ as the electrolyte component in anode cermets [5]. Kim et al. [6] studied the possibility of direct oxidation of sulfur-containing fuels with Cu-ceria-YSZ anodes. They demonstrated that Cu was not strongly affected by sulfur and Cu-ceria-YSZ anode was stable in 100 ppm sulfur at 973 K, while the cell performance declined in 5000 ppm sulfur because of the formation of Ce_2O_2S. Cu-ceria-YSZ anode has been studied for direct oxidation hydrocarbons [7,8] because Ni is very vulnerable to carbon poisoning. The combination of Cu and ceria is one of promising alternative cermet anodes since Cu is an excellent electric conductor and ceria is a well-known oxidation catalyst and has high ionic conductivity. One potential issue, however, was the extended morphological stability of Cu metal.

Applying oxides instead of cermets is alternative approach for anodes. Atkinson et al. [9], Jiang and Chan [10] discussed several oxide anode materials. Considering their redox stability, doped-ceria [11,12], Sc-Y-Zr-Ti-O [13], (La,Sr)(Cr,M)O_3 (M = Mn, Ru) [14,15], (Ba,Sr,Ca)(Ti,Nb)O_3 [16], doped $SrTiO_3$ and (La,Sr)TiO_x [17–20] could be potential candidates for alternative anodes. We have focused on doped $SrTiO_3$ as anode backbone component because, among these materials, doped $SrTiO_3$ has the highest known electrical conductivity in the anode gas environment [9,20]. $SrTiO_3$ is a chemically stable perovskite known to be a mixed ionic and electronic conductor (MIEC), and can be converted into an n-type semiconductor either by reduction or by doping with donors such as La^{3+}, Y^{3+} on the Sr-site and Nb^{5+} on the Ti-site. Hui and Petric [20] reported that Y-doped $SrTiO_3$ showed 80 S cm^{-1} at 1073 K in a reducing atmosphere ($P_{O_2} = 10^{-14}$ Pa), which is a typical anode condition for SOFCs.

The high performance of traditional Ni-YSZ anode in hydrogen depends significantly on the properties of the Ni because Ni performs multiple functions, including forming the electron conduction network, providing catalysis as well as giving structural integrity to the anode. An effective sulfur-tolerant anode material should be chemically and electrochemically stable, catalytically active, and electronically conductive at SOFC operating conditions, and it has been difficult to find an alternative that is better than Ni-YSZ. One approach is to separate the functions by replacing Ni with a mixed ionic–electronic conductor oxide and introduce as dispersed catalyst as shown schematically in Fig. 1. When using an electronically conductive material such as Ni, the triple phase boundary (TPB) is confined to the contact points between the electrode, electrolyte, and gas phase. Replacing Ni by an MIEC oxide and adding dispersed nano-sized catalytic materials increases this catalytically active area. The combination of a MIEC and dispersed catalysts might result in an acceptable performance even in sulfur-containing atmospheres.

Catalytic infiltration (or impregnation) is a common technique for polymer membrane fuel cell electrodes to disperse particles, and has recently been introduced for SOFC electrodes [21–24]. Jiang [25] recently reviewed the great potential of this technique in the development of nano-structure electrodes. The catalysts are usually introduced as liquid nitrates in already-formed porous electrodes. This method expands the range of choices for effective electrode materials combinations because of the elimination of thermal expansion mismatch and the suppression of possible deleterious reactions among the electrode and electrolyte materials during the membrane fabrication.

In the present study, Y-doped $SrTiO_3$ was chosen as a MIEC anode material combined with YSZ, and ceria or Ru were used as dispersed catalysts, to demonstrate highly sulfur-tolerant anodes since ceria and Ru are known as good anode catalyst [26–28]. The infiltrated anodes were evaluated in 10–40 ppm hydrogen sulfide balanced with hydrogen, at the temperatures between 973 and 1073 K. The effect of catalytic infiltration on the porous anode structure is discussed and potentially high-sulfur tolerant anodes were investigated.

2. Experimental

Prior to cell preparation, Y-doped $SrTiO_3$ powder was prepared by the Pechini method [29]. Titanium isopropoxide (Alfa Aesar) and citric acid (CA) (Alfa Aesar) were put in ethylene glycol (EG) (Alfa Aesar) in a mole ratio of Ti:CA:EG = 1:4:9.33 to make a Ti solution. The mixture was heated to 340–370 K on a hot plate and mixed with a stirrer to dissolve the CA powder. A sampling of the solution put into a crucible and fired at 1073 K for 14.4 ks to obtain an accurate Ti concentration of the

solution. The Ti concentration of the solution was calculated from the weight of the TiO_2 residual. The titanium solution was put in a Pyrex beaker, and heated to 340–370 K with a hot plate, and appropriate amounts of $SrCO_3$ (Alfa Aesar) and $Y_2(CO_3)_3{\cdot}xH_2O$ ($x \sim 3$) (Alfa Aesar) were introduced in the hot liquid slowly, since carbon dioxide release cause foaming. The solution was heated further to about over 573 K, and dried further under a heating lamp. The resulting solid was hand ground in a mortar and pestle, put in an alumina crucible, and pre-fired at 873 K for 14.4 ks to remove any residual carbon. After pre-firing, the powder was examined X-ray diffraction (XRD) with Cu Kα radiation, confirming that $Sr_{0.88}Y_{0.8}TiO_3$ (SYTO) had been synthesized.

Two types of cells were prepared. First, half-cells using a thick YSZ electrolyte disk (∼0.5 mm) were used to investigate the microstructure and properties of the Y-doped $SrTiO_3$-YSZ anodes, w/w infiltrated materials. A 20 g of 8 mol% Y_2O_3-doped ZrO_2 (Tosoh) was mixed with 2 wt.% of menhaden fish oil (MFO) (Sigma) as a binder and ∼50 ml isopropyl alcohol (IPA) (VWR), then ball milled with 3 mm zirconia milling balls (Union Process) for 86.4 ks. A binder containing 2 wt.% of poly(vinyl butyral-co-vinyl alcohol-co-vinyl acetate) (PVB) (Aldrich) and dibutyl phthalate (Mallinckrodt) as a plasticizer was added to the resultant solution and ball milled again for 3.6 ks. The solution was stirred and dried under a heat lamp. The resultant agglomerated YSZ was ground with a mortar and pestle, and passed through a 150 μm mesh sieve. The sieved YSZ powder was then uniaxially pressed into disks with a diameter of 38 mm at 103 MPa (15 kpsi) using a stainless steel die. The YSZ disks were sintered at 1673 K for 14.4 ks in air. To prepare anode suspension, 2 g of a SYTO-YSZ mixture in a weight ratio of 1:1 was attritor-milled with 0.1 g of MFO, 1 drop of dibutyl phthalate and 50 ml of IPA, using 3 mm zirconia milling balls for 3.6 ks, at 500 rpm. This anode suspension was ultrasonically dispersed and deposited onto the YSZ disks using aerosol spraying to form a thin anode layer with an area of 10 mm × 10 mm. The weight change of the disks was carefully measured during spraying to bring the anode thickness to 15–20 μm. The disks were then fired in a reducing atmosphere furnace with Ar–4%H_2 at a flow rate of 1 ml s^{-1} (60 ml min^{-1}), at 1573 K for 14.4 ks. For electrochemical testing, a Pt mesh current collector was attached with Pt paste to both sides of the disks, and reference electrodes were attached on the cathode side; then, the cell was fired at 1173 K for 1.8 ks to secure the Pt mesh to the cell.

Thin film, cathode-supported cells were prepared with Sr-doped lanthanum manganese oxide (LSM) to investigate the performance and sulfur tolerance of infiltrated SYTO-YSZ anodes. A mixture of LSM-YSZ was prepared with 10 g of YSZ powder (Tosoh), 10 g of $La_{0.65}Sr_{0.3}MnO_{3-\delta}$ powder (Praxair Specialty Ceramics), 2.5 wt.% of MFO, PVB and dibutyl phthalate. These materials were attritor-milled using YSZ balls, in IPA, for 3.6 ks, at 500 rpm. The suspension was then put in a beaker and 9 g of pore former; KS6 graphite (Timrex) was added with 2.5 wt.% of MFO, PVB and dibutyl phthalate. The solution was stirred and dried under a heating lamp. The resultant agglomerated LSM-YSZ was ground with a mortar and pestle, and passed through a 150 μm mesh sieve. The sieved LSM-YSZ powder was uniaxially pressed into disks with a diameter of 25 mm at 103 MPa (15 kpsi) using a stainless steel die, then pre-fired at 973 K for 14.4 ks in air. To prepare the electrolyte suspension, a mixture of 2 g of YSZ, 0.1 g of MFO, 1 drop of dibutyl phthalate and 50 ml of IPA, was attritor-milled for 3.6 ks, at 500 rpm. This suspension was used for depositing thin YSZ electrolytes (∼10 μm) onto the LSM-YSZ support by aerosol spraying. The resultant bilayers were sintered at 1573 K for 14.4 ks in air. The graphite in the cathode layer was burned out, leaving a porous LSM-YSZ cathode. The anode suspension of SYTO-YSZ was then ultrasonically dispersed, and sprayed onto the YSZ electrolyte to form a thin anode layer (15–20 μm) with an area of 7 mm × 7 mm. The resultant trilayer disks were sintered at 1473 K for 7.2 ks in air. Pt mesh current collectors were attached to the cathode and anode, and the assembled cell was fired at 1173 K for 1.8 ks to attach the Pt mesh.

A solution of ceria precursor was prepared by mixing 6.20 g of $Ce(NO_3)_3{\cdot}6H_2O$ (Alfa Aesar) and 0.3 g of a commercial polymeric dispersant, Triton-X (Union Carbide Chemical and Plastics Co., Inc.) with 1 ml of H_2O. The mixture was subsequently heated to about 373 K to produce a high concentrated solution. The precursor solution was infiltrated into the porous structure of SYTO-YSZ using a vacuum impregnation apparatus (Epovac, Struers), and pre-heated to 923 K for 1.8 ks in air to convert the precursor. A 0.1 M Ru solution also was prepared with $RuCl_3{\cdot}xH_2O$ ($x \leq 1$) (Sigma–Aldrich) and IPA. The Ru solution was infiltrated in the porous structure of SYTO-YSZ by using a microsyringe, then dried at room temperature.

The experimental setup for the sulfur tolerance test was constructed as shown in Fig. 2. The gas flow system consists of stainless steel tubes, flow controllers, valves and glass parts: a water vapor saturator and scrubber. About 3% of water vapor was added to the fuel gas by flowing the H_2 gas through the water vapor saturator at 298 K. Nitrogen was used to purge the system before H_2 and H_2S was introduced. A 10–40 ppm H_2S gas was generated by mixing a pure H_2 flow with a controlled flow of 50 ppm H_2S premixed H_2 gas. The total gas flow rate was fixed at 8.3×10^{-7} m^3 s^{-1} (50 ml min^{-1}). The cells were sealed onto a short alumina tube (height: 12 mm) with ceramic cement 552 (Aremco) to separate the cell from the test rig, so it could be used again after infiltration. The Pt mesh on anode side was connected to the inside Pt current collector wires using a spot welding machine, and the short alumina with the mounted cell tube was affixed to the test rig alumina tube. The gap between the short alumina tube and main alumina test rig tube was sealed with Aremco 552 cement. After drying the cement at room temperature, the completed test rig was placed in the isothermal zone of the furnace. The cell was heated to the curing temperatures of the ceramic cement, subsequently heated to 1073 K in rate of 0.05 K s^{-1} (3 K min^{-1}), and pre-treated at 1073 K in 3% humidified H_2 for 43.2 ks before electrochemical testing. The impedance spectra of the cells were measured under near-open circuit condition in the range of 0.1 Hz to 1 MHz by the combination of a Solartron frequency response analyzer 1255 and a Solartron electrochemical interface 1286, with 10 mV peak-to-peak applied ac voltage. The current–voltage (I–V) characteristics were measured between 973 and 1073 K, with an

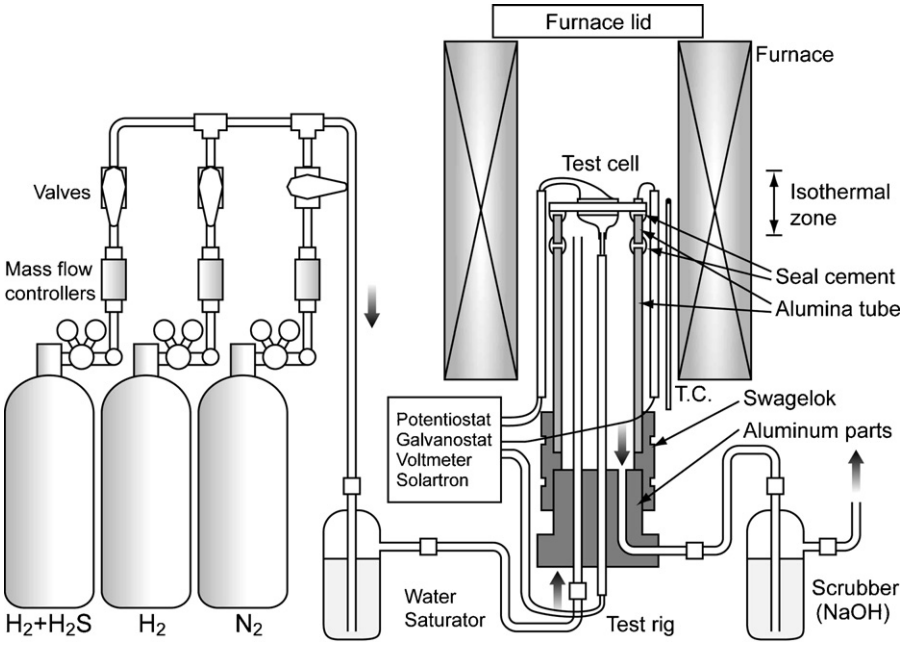

Fig. 2. Schematic diagram of experimental apparatus for sulfur-tolerant anode test.

Agilent 34970A data acquisition switch unit, and a Kepco BOP 20-5M bipolar power supply/amplifier. After electrochemical testing, the cells were fractured and the microstructures were examined with a Hitachi S-4300SE/N field emission scanning electron microscope (FE-SEM).

3. Results and discussion

3.1. Electrochemical properties and microstructures

In an alternative anode design such as shown schematically in Fig. 1, the dispersed catalysts in the anode structure play a very important role. The MIEC oxide of choice, Y-doped $SrTiO_3$ has high electric conductivity under anode conditions, but has no reported catalytic activity. The performance of the bare SYTO-YSZ anode must thus be enhanced by catalytic materials to be of practical use. The anodes deposited on the half-cells were examined in 3% humidified H_2. Fig. 3 shows the AC impedance spectra of these anode half-cells before and after infiltration. Both ceria and Ru infiltration significantly decrease the polarization resistance, and improve the cell performance while the Ohmic resistance was hardly changed, as shown in Fig. 3(a and b). The area-specific polarization resistance for the ceria-infiltrated cell was about 1.3 $\Omega\,cm^{-2}$ at 1073 K while that for non-infiltrated cell was about 2.6 $\Omega\,cm^{-2}$. The polarization resistance for the Ru-infiltrated cell was about 0.8 $\Omega\,cm^{-2}$, while that for non-infiltrated cell was about 2.6 $\Omega\,cm^{-2}$. Ru infiltration was also applied to ceria-infiltrated SYTO-YSZ. The combination of ceria and Ru infiltration decreased the polarization resistance of the cell drastically as shown in Fig. 3(c). The polarization resistance for the infiltrated cell was about 0.5 $\Omega\,cm^{-2}$ at 1073 K while that for non-infiltrated cell was about 2.9 $\Omega\,cm^{-2}$. These impedance plots showed that ceria and Ru were effective catalysts in the SYTO-YSZ anode.

The microstructures of the anodes of the half-cells were observed after impedance testing. Fig. 4 shows secondary electron micrographs of the anode microstructures of SYTO-YSZ, SYTO-YSZ with ceria infiltration and SYTO-YSZ with Ru infiltration. The particles of SYTO and YSZ were connected,

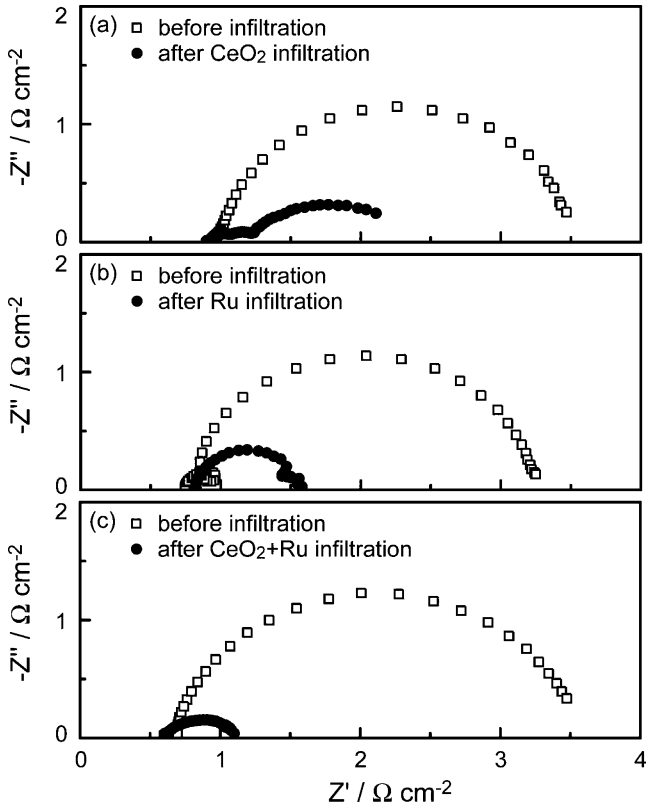

Fig. 3. Impedance spectra at 1073 K for the cells: (a) before and after the ceria infiltration, (b) before and after the Ru infiltration and (c) before and after the ceria and Ru infiltration.

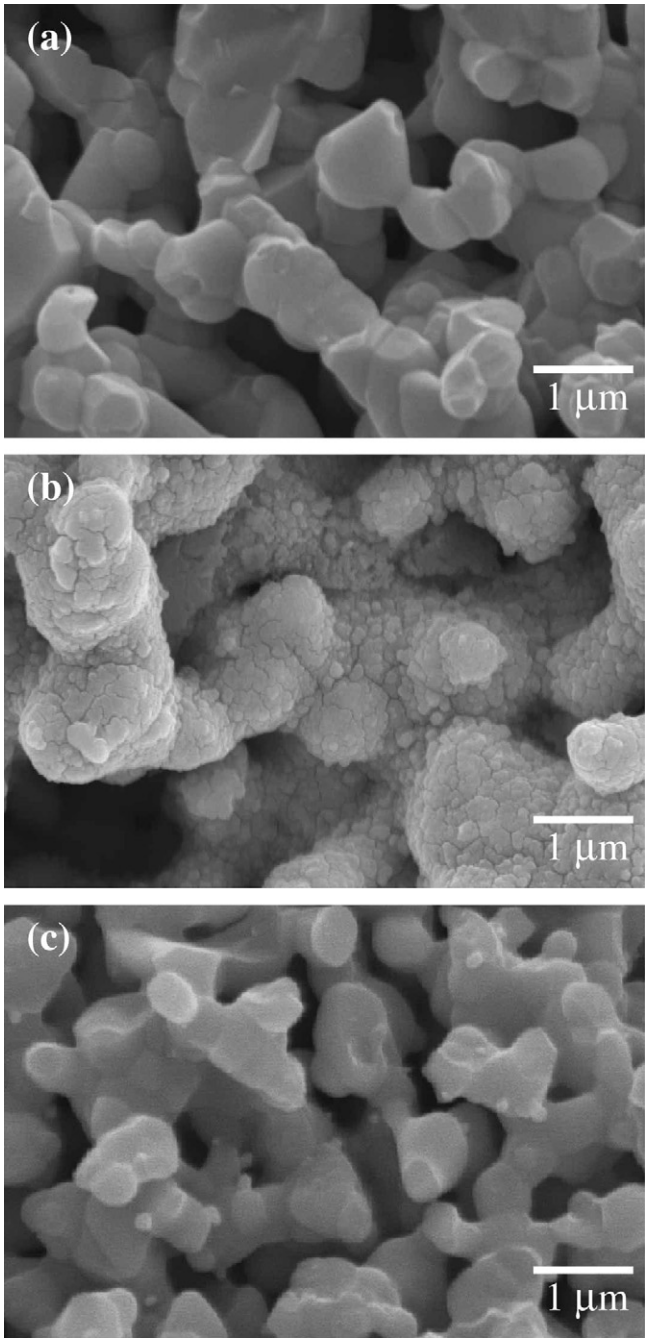

Fig. 4. Secondary electron micrographs of anode microstructures; (a) SYTO-YSZ, (b) SYTO-YSZ with ceria infiltration and (c) SYTO-YSZ with Ru infiltration.

forming a good network with appropriate porosity. The infiltrated ceria covered most of the pore walls of the SYTO-YSZ backbone, as shown in Fig. 4(b). The size of the ceria particles was 30–200 nm and the thickness of the layer was approximately 200 nm at the maximum. Assuming the porosity of the anode was 50%, the estimated volume ratio of ceria in the anode layer was 3.3 vol.%. Sholklapper et al. [24] reported that catalyst infiltration with nitrate by vacuum impregnation method could deposit 30–100 nm LSM particles on the walls of a porous YSZ cathode. Fig. 4(b) indicated that this technique could be applied effectively to ceria infiltration into porous anodes. The advantage of this method is not only that various kinds of sub-micron size oxides can be deposited effectively into porous electrodes, but also that it is a simple procedure. Ceria is well known as a catalytic material, and is a MIEC in reducing atmospheres as well. Placing mixed conducting materials as a continuous thin layer on the walls of the anode backbone extends both ionic and electronic character of the anode, making the whole wall surface catalytically active, leading to significant improvements in anode performance. Rare-earth elements can further be used doped to enhance the electrical and ionic conductivity of the ceria, as is known, e.g., for Sm-doped ceria (SDC) and Gd-doped ceria (GDC) [30]. Doped ceria has a high resistance to carbon deposition but its activity for hydrocarbon oxidation was lower than that of undoped ceria, and the requirement for adding an active oxidation catalyst has been proposed [12]. Since undoped-ceria infiltration already decreased the polarization resistance of SYTO-YSZ anode, an alternative anode using with doped ceria infiltration may improve performance even more.

Introducing a second active catalyst onto the thin ceria layer is another option for further improving the anode performance. The impedance spectra of ceria and Ru dually infiltrated SYTO-YSZ anodes support this idea as shown in Fig. 3(c). We used Ru as a dispersed catalyst because it is known as a good catalyst for hydrogen oxidation and hydrocarbon oxidation. Suzuki et al. [26] demonstrated that the Ru/YSZ cermet has a high catalytic activity and a high resistance to carbon deposition. They reported that the polarization resistance of Ru/YSZ cermet was smaller than that of Ni/YSZ at 1273 K. Sun et al. [27] investigated flowerlike, mesoporous ceria-Ru as a reforming catalyst layer and reported that a pronounced performance improvement was observed when a catalyst layer was added on a Ni-SDC anode layer. Zhan and Barnett [28] examined the effect of a ceria-Ru catalyst layer in combination with traditional anodes, Ni-YSZ and Ni-SDC, and reported that the catalyst layer allowed internal reforming of iso-octane without coking. Though the ceria-Ru catalyst layer showed very good performance for hydrocarbons, they described also three drawbacks of the catalyst layer: reduced fuel diffusion to the anode, current collection problems and the cost of Ru. However, applying a low catalyst loading by infiltration in non-Ni based anode structures such as SYTO-YSZ can remove these drawbacks for the ceria-Ru catalyst.

Small particles of Ru were observed on SYTO-YSZ network as shown in Fig. 4(c). The size of the particles was 30–200 nm and the particles were dispersed onto the pore walls of the anode backbone. The amount of Ru particles was low because the concentration of the precursor was 0.1 M, and the estimated volume ratio of Ru in the anode layer was only 0.04 vol.%. Yet, infiltrated Ru improved significantly the cell performance as shown Fig. 3(b) in spite of this very low loading. Though Ru is one of noble metals, the current price is relatively low among the platinum-group noble metals as shown in Table 1. In the infiltration method, the necessary amount of Ru for a 1 cm^2 anode area is at most 1 μmol. If a cell would operate at power density of only 100 mW cm^{-2}, the cost metallic Ru for 1 kW stack is only US$ 1.85. Catalyst infiltration with Ru can therefore be a

Table 1
Price of platinum-group metals

	Price/US$ (oz t)$^{-1}$ [a]	Molecular weight	Cost for 1 mol / US$	Cost for 1 kW / US$ (in case of 100 mW cm^{-2})
Platinum, Pt	852	195.08	5344	53.44
Palladium, Pd	252	106.42	862	8.62
Rhodium, Rh	736	102.91	2435	24.35
Ruthenium, Ru	57	101.07	185	1.85

[a] Quoted from Ref. [31], oz t: troy ounce = 31.1035 g.

cost-effective method to improve the catalytic performance of anodes.

The cathode support cells with ceria- and Ru-infiltrated SYTO-YSZ anode were prepared to investigate the sulfur tolerance of the anode. Fig. 5 shows current–voltage characteristics and power density of a cathode support cell with ceria- and Ru-infiltrated SYTO-YSZ anode at 973–873 K in 3% humidified H_2. The peak power density of the cell was 510 mW cm^{-2} at 1073 K, at 0.85 mA cm^{-2} and 240 mW cm^{-2} at 973 K, at 0.5 mA cm^{-2}. The impedance spectra of the cells were measured at 1073 K in humidified H_2, and in humidified $H_2 + H_2S$ mixtures as shown in Fig. 6. Two arcs were observed in the spectra, and the summit frequencies of the high and low frequency arcs were 1 kHz and 13 Hz, respectively. Though the analysis of impedance spectra of multi-player fuel cells is complicated, the low frequency arc is generally considered to be associated with a gas diffusion and conversion processes [32], while the high frequency arc is considered to be related to charge transfer process of electrodes. The size of the high frequency arcs did not change very much, while that of low frequency arcs changed by the presence of H_2S. The size of the low frequency arc was increased by 5, 8 and 21% in 10, 20 and 40 ppm H_2S, respectively (an arc fitting calculation was carried out between 1 and 100 Hz to obtain these values). The polarization resistance of the anode quickly changed after H_2S was introduced because the arcs at 1.2 and at 3.6 ks were almost the same. After the cell was exposed to 10 ppm H_2S for 3.6 ks, H_2S gas was stopped and the low frequency arc of the impedance spectra was completely recovered within 10.8 ks, while the arc did not recover completely within 10.8 ks in the case of 40 ppm. For comparison, for a Ni-YSZ anode the polarization resistance almost doubled in response to only a 1 ppm H_2S contamination at 1173 K, and took 90 ks to recover [4]. The SYTO-YSZ anode with ceria and Ru infiltration clearly showed a superior sulfur tolerance compared to conventional Ni-YSZ anodes. Though the infiltrated SYTO-YSZ anode materials must be stable and cannot react with H_2S, the impedance was increased and recovered quickly in the ppm-level H_2S atmospheres. This phenomenon might be associated with the reversible adsorption of gaseous sulfur species, which block active triple phase boundaries for oxidation of hydrogen.

A constant current was applied to check stability of the cell in the 10 ppm H_2S/H_2 atmosphere. The cell voltage was monitored under a fixed current density of 0.5 A cm^{-2}, and the fuel atmosphere was changed as shown in Fig. 7. The cell voltage quickly dropped only from 0.79 to 0.78 V in 1.6 ks when H_2S was added to hydrogen and the cell voltage recovered in ~4 ks after H_2S

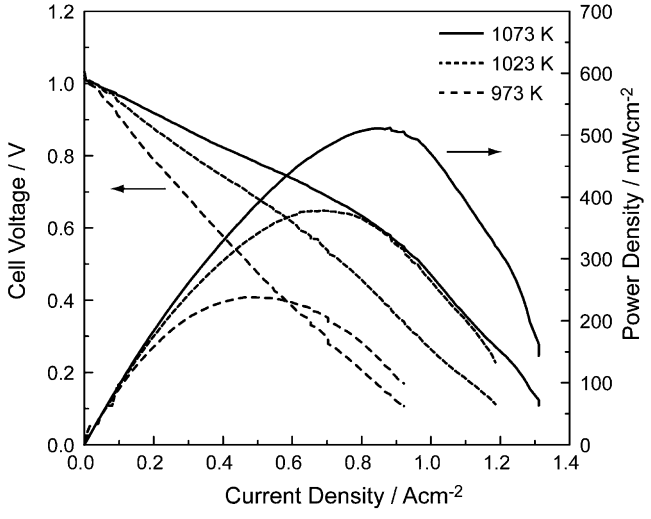

Fig. 5. Cell voltage and power density as a function of current density for a cathode support cell with ceria- and Ru-infiltrated SYTO-YSZ anode at 973–873 K.

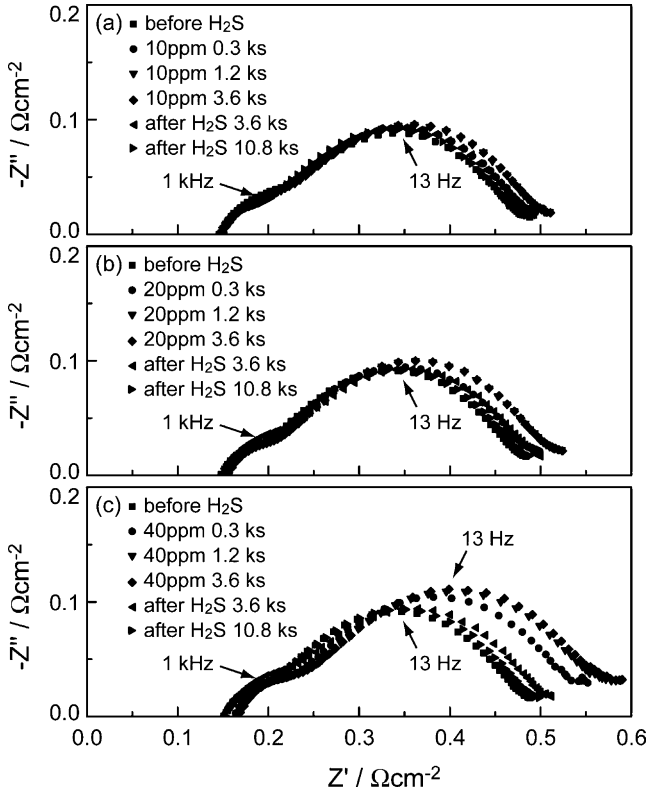

Fig. 6. Impedance spectra at 1073 K for a cathode support cell with ceria- and Ru-infiltrated SYTO-YSZ anode, (a) 10 ppm H_2S, (b) 20 ppm H_2S and (c) 40 ppm H_2S.

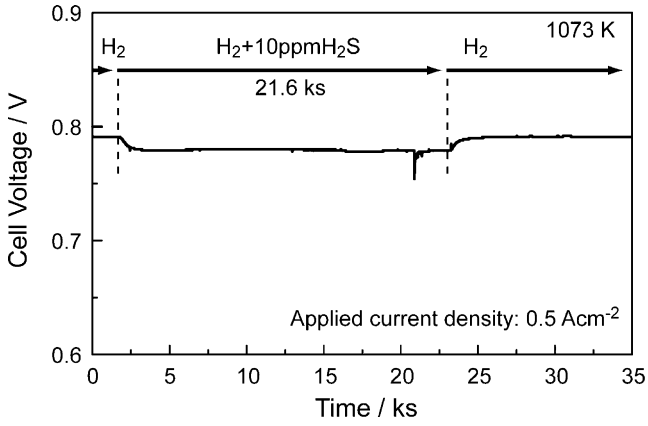

Fig. 7. Cell voltage as a function of time for a cell exposed to 10 ppm H_2S at 1073 K.

was stopped. These degradation and recovery times correspond to the impedance spectra of Fig. 6(a). Note though that the recovery time was longer than the degradation time. Fig. 8 shows current–voltage characteristics and power density of the cell exposed to 10 ppm H_2S at 1073 K. The peak power density of the cell dropped slightly from 510 to 470 mW cm^{-2} after H_2S was added. The current–voltage characteristics was constant from 10.8 to 21.6 ks during H_2S exposure, and it almost recovered in 10.8 ks after H_2S stopped even though the power density curve was very slightly shifted to the right. Figs. 7 and 8 indicate that the performance of ceria- and Ru-infiltrated SYTO-YSZ anode did not decline very much in 10 ppm H_2S under current. The microstructure of the cathode support cell was observed after the sulfur test as shown in Fig. 9. The thickness of the electrolyte and anode layer was about 10 and 20 μm, respectively, and both electrode layers have appropriate porosity for gas diffusion as shown in Fig. 9(a). In the anode layer, very small particles covered the SYTO-YSZ backbone, as shown in Fig. 9(b). It was difficult to distinguish ceria and Ru, but according to Fig. 4, most of particles must be ceria and only some particles would be Ru.

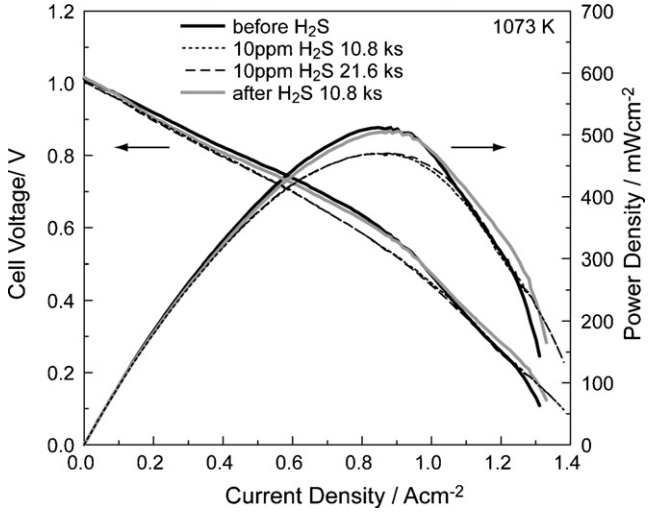

Fig. 8. Cell voltage and power density as a function of current density for a cell exposed to 10 ppm H_2S at 1073 K.

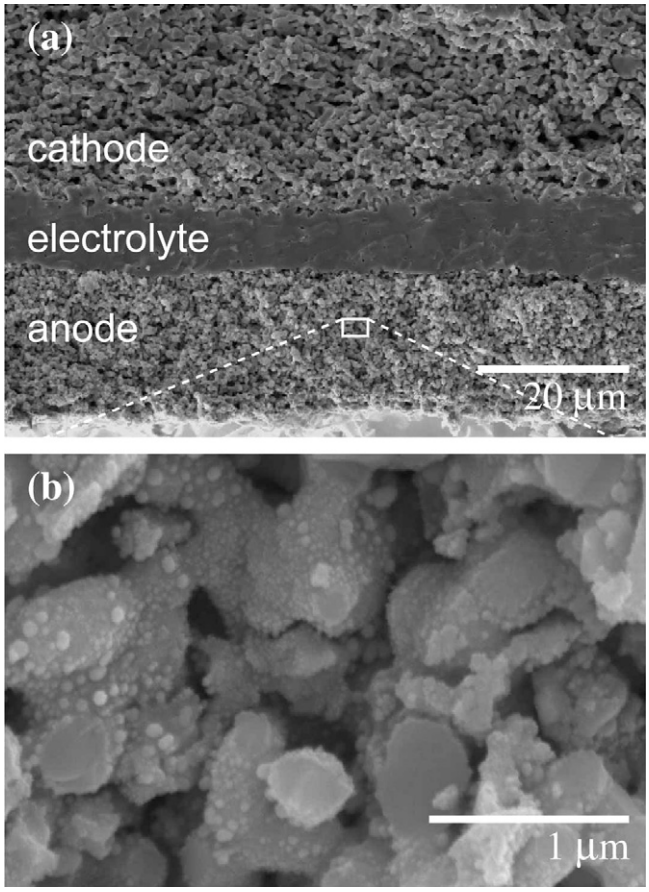

Fig. 9. Secondary electron micrographs of cathode support cell tested in H_2S conditions.

Significant voltage drop for Ni-based anodes exposed to ppm-level H_2S was reported by Sasaki et al. [5], e.g., the voltage of a cell with Ni-YSZ anode dropped by about 0.5 V in 5 ppm H_2S at 0.2 A cm^{-2}, at 1123 K. In general, 5–10 ppm is the maximum amount of sulfur-containing compounds (added intentionally as an odorant) for natural gas. This exceeds the tolerance of traditional Ni-YSZ anodes. Sulfur removers need then to be incorporated in the SOFC system, when odorized natural gas is contemplated as a fuel for SOFCs with conventional Ni-YSZ anode. If cost-effective high sulfur tolerant anodes were used as described here, sulfur removal is not needed, allowing a significant system cost reduction. In the present study, ceria- and Ru-infiltrated SYTO-YSZ anode showed much higher sulfur tolerance than traditional Ni-YSZ anodes, and demonstrated the possibility of MIEC-YSZ anode and nano-sized catalytic infiltrations for SOFCs.

3.2. *Chemical stability of nano-sized catalysts*

The MIEC oxide for the anode structure, Y-doped $SrTiO_3$ must be stable in SOFC anode conditions including ppm-level sulfur since each single element of the material (Y, Sr and Ti) does not react with sulfur in the anode conditions. But the chemical stability of the dispersed catalysts should be discussed since the size of the catalysts was very small, and reaction with sul-

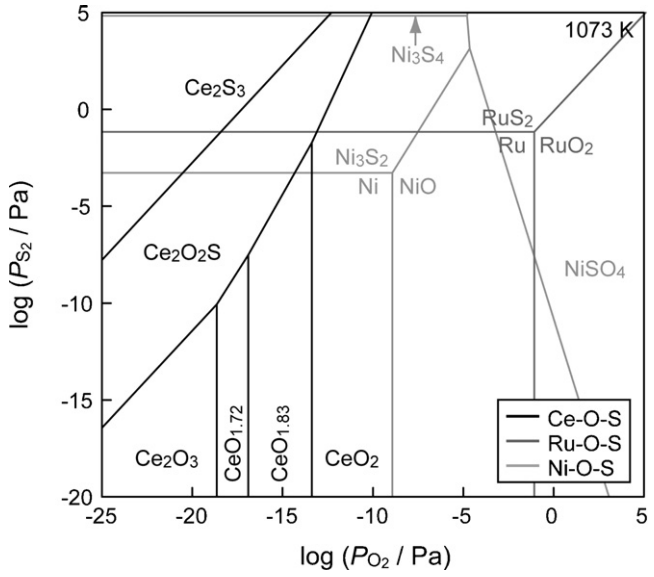

Fig. 10. Phase stability diagrams of M–O–S (M = Ce, Ru and Ni) at 1073 K.

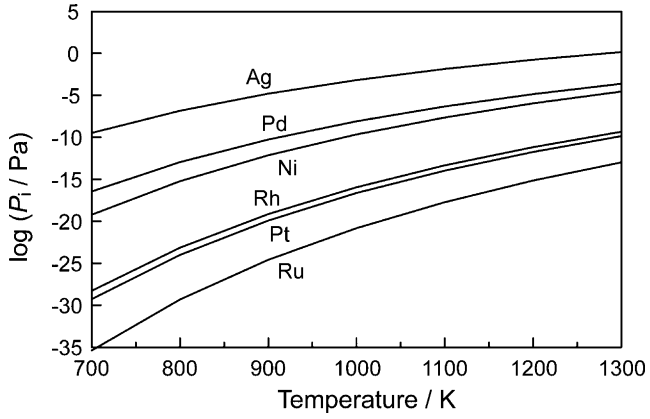

Fig. 11. Partial pressures of catalytic metals.

fur could be detrimental. Ferrizz et al. [33] investigates Ce–O–S phase diagrams between 873 and 1073 K, and reported that the formation of Ce_2O_2S requires higher sulfur partial pressures than suggested in previous studies, especially at lower temperatures. Phase stability diagrams of Ru–O–S and Ni–O–S were calculated from available thermodynamic data [34], and compared with reported Ce–O–S diagram [33] at 1073 K as shown in Fig. 10. The oxygen partial pressure range of typical SOFC anode conditions corresponding to $H_2/H_2O = 97/3$–$10/90$ (inlet–outlet) is $\log(P_{O_2}/\mathrm{Pa}) = -16.4$ to -11.5 at 1073 K. In this oxygen partial pressure range, cerium should exist as Ce_2O_2S at higher sulfur and low oxygen partial pressure. Kim et al. [6] reported that the cell performance with Cu-ceria-YSZ anode was stable in 100 ppm sulfur for 360 ks while it declined in 5000 ppm sulfur. The phase diagrams of M–O–S should be used carefully because the actual P_{S_2} in the anode is usually much less than the P_{H_2S}. Kim et al. reported that the actual values of the P_{S_2} were much lower than the P_{H_2S} ones, and the experimental results for ceria stability were in agreement with the phase stability diagram. In the present study, the equilibrium partial pressure of S_2, P_{S_2}, was estimated from the reactions: $H_2S + \frac{3}{2}O_2 = SO_2 + H_2O$ and $S_2 + 2O_2 = SO_2$ from thermodynamic data [33], and was about 10^{-9} Pa at 10 ppm H_2S, at 1073 K. Ceria catalyst must be stable in ~40 ppm H_2S, and the effect of sulfur on the performance ceria-based catalysts under reducing conditions should be negligible small in low sulfur conditions. Partial pressure of sulfur, P_{S_2}, at the phase boundary of Ru/RuS_2 is 6.9×10^{-2} Pa while that of Ni/Ni_3S_2 is 5.3×10^{-4} Pa, as shown in Fig. 10. In addition, it should be noted that Ni_3S_2 is liquid at 1073 K [35] while RuS_2 is solid [34]. Shatynski [35] studied transition metal sulfides, and reported on nickel sulfides; the melting point of Ni_3S_2 and NiS_2 is 1063 and 1281 K, respectively, while Ni_3S_4 decomposes at 629 K. Formation of liquid Ni_3S_2 would deteriorate Ni-YSZ anode performance rapidly. In 10 ppm H_2S at 1073 K, Ni must react with sulfur and formation of liquid sulfide will deteriorate the Ni–YSZ microstructure. Infiltrated nano-sized ceria and Ru particles were observed even after significant sulfur exposure, as shown in Fig. 9: these materials keep their structure in sulfur conditions. The diagrams indicate that Ru is more stable than Ni in sulfur conditions since the phase boundary of Ru/RuS_2 is at about 2 orders of magnitude higher sulfur partial pressure than for Ni/Ni_3S_2. As shown in Fig. 3, the polarization resistance of ceria- and Ru-infiltrated anode increased quickly and completely recovered for 10 ppm H_2S. The calculated equilibrium partial pressure of S_2 of 10 ppm H_2S condition at 1073 K was about 10^{-9} Pa, much lower than the P_{S_2} at the phase boundary of Ru/RuS_2. It may be concluded that Ru was thermodynamically stable in the present conditions.

In addition to stability in sulfur, agglomeration and vaporization should be discussed for Ru. The melting point of Ru is much higher (2523 K) than Ni (1728 K) [34], and therefore Ru is significantly less prone to sintering than Ni [26]. The estimated amount of Ru particles was only 0.04 vol.% as shown in Fig. 4(c), and this dispersion does not cause agglomeration of Ru. Vaporization of Ru could also be a concern because nano-sized particles would disappear if the vaporization rate is high at operating temperatures. Partial pressures of potential catalytic metals were calculated from thermodynamic data [36] as shown in Fig. 11. The partial pressure of Ru is the smallest among the catalytic metals (Pt, Pd, Rh, Ru, Ni and Ag), and vanishingly small at operating temperatures of SOFCs. These low values of partial pressures should allow long-term stability of nano-sized Ru particles.

As a consequence, the infiltrated catalysts ceria and Ru have higher sulfur tolerance than Ni and are stable at ppm levels of sulfur. As described above, the maximum amount of sulfur-containing odorant for natural gas is 5–10 ppm. Ceria and Ru are therefore promising sulfur tolerant anode catalysts for SOFCs that are operated with natural gas or hydrocarbon gases containing sulfur odorants.

4. Conclusions

A sulfur tolerant SOFC anode was demonstrated for 10–40 ppm H_2S fuel streams. The anodes were composed of Y-doped $SrTiO_3$ infiltrated with ceria and Ru. The infiltrated cat-

alytic materials, ceria and Ru, decreased the polarization resistance of SYTO-YSZ anode respectively and the combination of these two materials improved the anode performance significantly. A cathode supported cell with ceria- and Ru-infiltrated SYTO-YSZ anodes showed a constant maximum power density 470 mW cm^{-2} in 10 ppm H_2S/H_2 at 1073 K. Dispersed nano-sized ceria and Ru particles were stable in such sulfur-containing fuels. The sulfur tolerance of the ceria- and Ru-infiltrated SYTO-YSZ anode was much higher than that of traditional Ni-YSZ anodes. The present study indicates the possibility of using cost-effective MIEC-YSZ anodes with infiltrated nano-sized catalytic materials as sulfur tolerant anodes of SOFCs.

Acknowledgment

This work was supported by the U.S. Department of Energy under Contract No. DE-AC02-05CH11231.

References

[1] N.Q. Minh, T. Takahashi, Science Technology of Ceramic Fuel Cells, Elsevier, 1995, p. 209.
[2] J. Geyer, H. Kohlmüller, H. Landes, R. Stübner, in: U. Stimming, S.C. Singhal, H. Tagawa, W. Lehnert (Eds.), Solid Oxide Fuel Cells (SOFC), vol. V, The Electrochemical Society, Pennington, NJ, 1997, p. 585, PV97-40.
[3] S. Primdahl, M. Morgensen, in: S.C. Singhal, M. Dokiya (Eds.), Solid Oxide Fuel Cells (SOFC), vol. VI, The Electrochemical Society, Pennington, NJ, 1999, p. 530, PV99-19.
[4] Y. Matsuzaki, I. Yasuda, Solid State Ionics 132 (2000) 261.
[5] K. Sasaki, K. Susuki, A. Iyoshi, M. Uchimura, N. Imamura, H. Kusada, Y. Teraoka, H. Fuchino, K. Tsujimoto, Y. Uchida, N. Jingo, in: S.C. Singhal, J. Mizusaki (Eds.), Solid Oxide Fuel Cells (SOFC), vol. IX, The Electrochemical Society, Pennington, NJ, 2005, p. 1267, PV2005-07.
[6] H. Kim, J.M. Vohs, R.J. Gorte, Chem. Commun. 2001 (2001) 2334.
[7] R.J. Gorte, H. Kim, J.M. Vohs, J. Power Sources 106 (2002) 10–15.
[8] S. Park, J.M. Vohs, R.J. Gorte, Nature 404 (2000) 256.
[9] A. Atkinson, S. Barnett, R.J. Gorte, J.T.S. Irvine, A.J. Mcevoy, M. Mogensen, S.C. Singhal, J. Vohs, Nat. Mater. 3 (2004) 17.
[10] S.P. Jiang, S.H. Chan, J. Mater. Sci. 39 (2004) 4405.
[11] E.R-. Cabrera, A. Atkinson, D. Chadwick, Appl. Catal. B: Environ. 47 (2004) 127.
[12] O.A. Marina, M. Mogensen, Appl. Catal. A: Gen. 189 (1999) 117.
[13] S. Tao, J.T.S. Irvine, J. Solid State Chem. 165 (2002) 12.
[14] S. Tao, J.T.S. Irvine, Nat. Mater. 2 (2003) 320.
[15] A.-L. Sauvet, J. Fouletier, J. Power Sources 101 (2001) 259.
[16] P.R. Slater, J.T.S. Irvine, Solid State Ionics 120 (1999) 125.
[17] P.R. Slater, D.P. Fagg, J.T.S. Irvine, J. Mater. Chem. 7 (1997) 2495.
[18] J. Canales-Vázquez, S.W. Tao, J.T.S. Irvine, Solid State Ionics 159 (2003) 159.
[19] O.A. Marina, N.L. Canfield, J.W. Stevenson, Solid State Ionics 149 (2002) 21.
[20] S.Q. Hui, A. Petric, J. Electrochem. Soc. 149 (2002) J1.
[21] S.P. Jiang, Y.J. Leng, S.H. Chan, K.A. Khor, Electrochem. Solid-State Lett. 6 (2003) A67.
[22] Y. Huang, J.M. Vohs, R.J. Gorte, J. Electrochem. Soc. 151 (2004) A646.
[23] K. Yamahara, C.P. Jacobson, S.J. Visco, L.C. De Jonghe, Solid State Ionics 176 (2005) 275.
[24] T.Z. Sholklapper, C. Lu, C.P. Jacobson, S.J. Visco, L.C. De Jonghe, Electrochem. Solid-State Lett. 9 (2006) A376.
[25] S.P. Jiang, Mater. Sci. Eng., A 418 (2006) 199.
[26] M. Suzuki, H. Sasaki, S. Otoshi, A. Kajimura, M. Ippommatsu, Solid State Ionics 62 (1993) 125.
[27] C. Sun, Z. Xie, C. Xia, H. Li, L. Chen, Electrochem. Commun. 8 (2006) 833.
[28] Z. Zhan, S.A. Barnett, Science 308 (2005) 844.
[29] M.G. Pechini, U.S. Patent 3,330,697 (1967).
[30] H. Inaba, H. Tagawa, Solid State Ionics 83 (1996) 1.
[31] U.S. Geological Survey, Mineral Commodity Summaries, January 2005.
[32] S.P. Yoon, S.W. Nam, J. Han, T. Lim, S. Hong, S. Hyun, Solid State Ionics 166 (2004) 1.
[33] R.M. Ferrizz, R.J. Gorte, J.M. Vohs, Appl. Catal. B: Environ. 43 (2003) 273.
[34] O. Knacke, O. Kubaschewski, K. Hesselmanneds (Eds.), Thermochemical Properties of Inorganic Substances, second ed., Springer-Verlag, Berlin, 1991.
[35] S.R. Shatynski, Oxid. Met. 11 (1977) 307.
[36] I. Barin, Thermochemical Data of Pure Substances, third ed., VCH Verlagsgesellschaft, Weinheim, 1995.